

Elucidating the Role of Distinct Mass Transport Processes in Redox Flow Batteries

A thesis proposal submitted by:

[REDACTED]

Date of Submission: October 25th, 2017

Date of Presentation: November 15th, 2017

Thesis Adviser: Fikile R. Brushett

Thesis Committee:

Fikile R. Brushett

[REDACTED]
[REDACTED]

William M. Deen

[REDACTED]
[REDACTED]



Paula T. Hammond

[REDACTED]
[REDACTED]

Table of Contents

List of Figures	ii
List of Tables	ii
1. Specify Aims	1
2. Background	2
2.1. Motivation	2
2.2. Redox Flow Batteries Overview	2
2.2.1. Vanadium Flow Batteries	3
2.2.2. Non-aqueous Redox Flow Batteries	3
2.3. Losses in Redox Flow Batteries	4
3. Research Plan	7
3.1. Understanding Role of Electrode Morphology on Performance	7
3.2. Transport at Each Position in Porous Electrodes	9
3.3. [REDACTED]	10
3.4. Distinct Mass Transport Mechanisms in Operating Flow Cells	12
3.4.1. System Design and Validation	12
3.4.2. Mechanistic Contributions to Electrolyte Crossover	13
4. Safety	14
5. Timeline	15
6. References	16

List of Figures

Figure 2.1: RFB Schematic	2
Figure 2.2: Molecular and separator design strategies	4
Figure 2.3: Flow field configuration	5
Figure 2.4: Convective, diffusive, and migrative flux	6
Figure 3.1: Characterization and performance of heat treated SGL 29AA	8
Figure 3.2: In-plane and through-plane orientation	10
	
Figure 3.4: Molecular structure of oxidized	11
	
Figure 3.6: Crossover flow cell configuration	12

List of Tables

<u>Table 5.1</u> : Proposed thesis timeline	15
---	----

1. Specify Aims

The aims begin with a brief introductory paragraph

The electricity grid is in desperate need of infrastructure innovations to meet the world's growing demand for energy. Energy storage can help address these needs by increasing grid reliability, lowering electricity costs, and deferring the need for grid infrastructure repairs.¹ Redox flow batteries (RFBs) are a promising technology for energy storage, offering independent scaling of energy and power; however, cost reductions are necessary for widespread implementation. To meet cost targets, cell performance must be improved. We can achieve significant advances by addressing gaps in our knowledge of RFB processes. In particular, transport within RFBs is poorly understood: RFB transport processes are multiscale and multivariate, making characterization challenging. Further, the effect of each mechanism is difficult to separate and study independently. My research will focus on deconvoluting the effect of RFB transport processes to understand how transport mechanisms can be manipulated to improve performance.

Electrodes govern reaction kinetics and system power, and optimizing electrodes can lead to vast improvements in RFB performance.² Liquid electrolyte is distributed within porous electrodes via multiple transport processes such as convection and diffusion, hence transport is important to reaction utilization and cell efficiency. Therefore, the first question my thesis will address is:

1. What is the role of surface composition, morphology, and electrolyte properties on transport within porous electrodes?

To address this question, I will study electrodes with a combination of ex situ characterization techniques and in situ performance analysis. [REDACTED]

[REDACTED] Current RFBs utilize fibrous carbon gas diffusion layers as electrodes, which were originally designed for gas transport in fuel cells and as such have potential for optimization for use in liquid phase RFB systems. The knowledge of optimal electrode properties gained in answering this first question can be used to design electrodes specifically for optimal transport of RFB electrolytes.

Separators are also essential to cell performance, as they are necessary to maintain electroneutrality. However, active species crossover through the separator is the primary cause of limited Coulombic efficiency and capacity fade.³ Separators that effectively block active species transport are essential for high efficiencies and long lifetime. Ion exchange membranes (IEMs) such as Nafion are most commonly used in RFBs. IEMs are designed to conduct one ion; however, they allow crossover when active species share the same charge as the target ion, or when ionic strength of oppositely charged species overcomes Donnan exclusion.⁴ These shortcomings motivate research into alternative separators. One promising substitute are size selective separators, which block materials with larger molecular radii while allowing unhindered flow of all other species regardless of charge. This alteration in function influences the transport mechanisms causing crossover, which I will study by addressing the following question:

2. What are the impacts of diffusion, convection, and electromigration on crossover and subsequent flow cell performance and how can these effects be experimentally deconvoluted?

I will begin by studying crossover of active species of varying [REDACTED] in a lab scale flow cell architecture to understand the effect of [REDACTED] RFB performance. To deconvolute the contribution of individual transport mechanisms, I will utilize a novel flow cell architecture where convective contributions to crossover can be measured separately from diffusive and electromigrative contributions. Identifying dominant contributions to crossover will allow us to seek strategies to prevent it. This understanding can be exploited for more efficient system design that can lead to widespread implementation of RFBs for grid energy storage.

Each aim is set apart from the rest of the text

Each aim is concisely stated in one sentence, followed by a longer description

2. Background

The background begins with a brief overall motivation, to orient the reader

2.1. Motivation

Increased utilization of energy storage is essential to meet projected energy needs. According to the United States Department of Energy, U.S. energy demand will be 4-5 TWh by 2050.¹ Massive grid expansion and diversified energy sources such as renewables will be required to meet energy demands. Energy storage can increase efficiency of the current grid infrastructure, delaying the need for repairs.^{1,5} Storage can allow integration of intermittent renewable resources such as solar or wind, and the increased use of renewables will reduce fossil fuel dependence and decrease greenhouse gas emissions.⁶ Energy storage is currently underexploited: in 2013, the U.S. was capable of storing only 2.3% of its total energy production.¹ The most utilized storage technology is pumped hydro, but deployment has stagnated due to geographical constraints.⁷ Before widespread grid scale energy storage can be implemented, there are several objectives that must be met, including reducing system cost and increasing safety and lifetime.¹ Redox flow battery (RFB) technology has great potential to meet these requirements. RFBs have inherent advantages for large scale stationary storage applications: energy and power can be scaled independently, allowing capacity and power demand to be met exactly.⁸ Additionally, liquid phase chemistries avoid growth of metal dendrites, making them safer than solid state batteries such as lithium ion.⁹ However, there is still progress to be made before RFBs see ubiquitous adoption. The U.S. DOE has set an aggressive cost target of \$150/kWh for RFBs;¹ however, models show that for optimized state of the art systems with 4 hour discharge capacity, current system costs are \$350/kWh.¹⁰ Deeper understanding of RFB design and operation are necessary to ensure systems can meet both cost objectives.

2.2. Redox Flow Batteries Overview

The background uses sections to improve readability

A typical flow battery configuration is shown in Figure 2.1. Positive and negative electrolyte are stored externally and pumped into their respective half-cells. During discharge the negative species is oxidized and donates an electron that travels through an external circuit to the positive electrode, where the positive species is reduced and gains an electron. During charge, the Faradaic reactions are reversed and current flows from negative to positive electrode. The electrodes are separated by a separator that allows transport of supporting ions, maintaining electroneutrality.

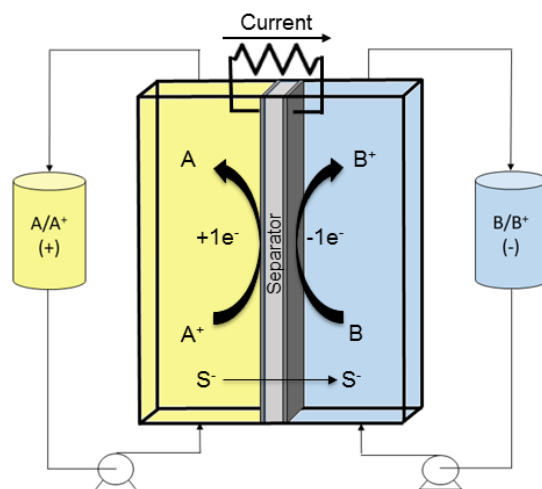
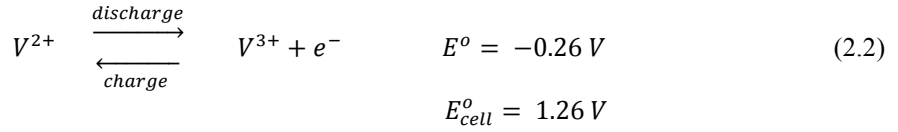
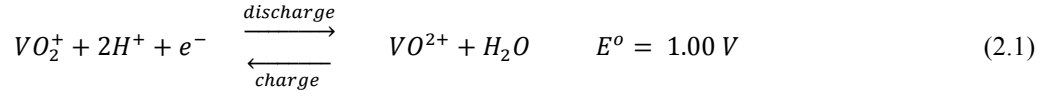


Figure 2.1: RFB schematic. The above configuration shows a discharge process. Idealized separator function allows transport of supporting anion, S^- , but prevents crossover of active species.

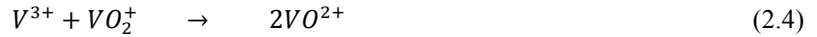
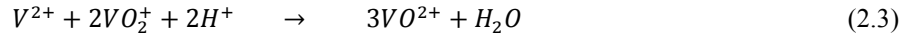
2.2.1. Vanadium Flow Batteries

Currently, vanadium redox flow batteries (VRBs) are the state of the art in RFB technology, and are the most widely commercialized flow battery chemistry.¹¹ VRBs utilize vanadium as both the positive

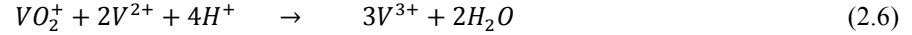
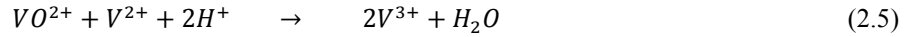
and negative active species. The positive and negative redox couples are given in Equations (2.1) and (2.2), respectively.¹² VO_2^+ is the V(V) oxidation state, and VO^{2+} is the V(IV) oxidation state.



The benchmark separators used in a VRB are Nafion membranes.¹³ Nafion incorporates sulfonate groups onto a Teflon backbone. It is acid resistant and has high proton conductivity, making it ideal for use with acidic RFB chemistries.¹⁴ However, Nafion is semi-permeable and permits transport of vanadium ions and water. The driving transport mechanisms of crossover will be discussed in Section 2.3.2. When V^{2+} and V^{3+} cross over to the positive electrode, reactions (2.3) and (2.4) occur¹⁵:



When VO^{2+} and VO_2^+ cross over to the negative side, reactions (2.5) and (2.6) take place¹⁵:



A key advantage of VRBs is that crossover does not cause irreversible capacity fade: mixing electrolytes will result in a solution of 50% V^{3+} and 50% V^{4+} , restoring original electrolyte capacity. However, remixing requires battery systems to be taken offline⁴ and necessitates an initial charging step to oxidize V^{3+} to V^{4+} at the positive electrode and reduce V^{4+} to V^{3+} at the negative electrode.¹⁶

Vanadium redox reactions are sluggish on carbon electrodes, and as such this system can be used to investigate the impact of electrode morphology on both kinetics and transport. The ability to study both kinetic and transport effects makes vanadium a model system I will utilize throughout my thesis work.

2.2.2. Non-aqueous Flow Batteries

Aqueous electrolytes have thermodynamically limited operating voltage windows of about 1.23 V: at 0 V vs standard hydrogen electrode (SHE) redox reactions compete with the hydrogen evolution reaction (HER), while at 1.23 V vs. SHE reactions compete with oxygen evolution (OER).¹⁷ Non-aqueous flow batteries (NAqRFBs) utilize organic solvents that avoid these reactions and so allow wider voltage windows. Many classes of electrolyte materials have been investigated for NAqRFBs, including organic molecules, metal centered coordination complexes, and suspended particulates.¹⁸ Organics are particularly advantageous for the ability to promote desired properties such as solubility, conductivity, and redox potential through molecular engineering. Organic active species can be bound to polymer or oligomer chains. The increased molecular radius of these redox active oligomers (RAOs) or polymers (RAPs) permit the use of a porous separator in place of an IEM, significantly reducing system cost.⁸ Porous separators prevent crossover by hindering transport of large ions.¹⁹ Larger molecular size inhibits crossover, but increasing molecular weight reduces solubility, limiting energy density. Additionally, larger molecules often have higher viscosity in solution, increasing system pumping cost.²⁰ Further study is needed to elucidate solution phase behavior of RAOs, and a research plan is discussed in Section 3.3.

Active species design must be coupled with separator design for effective crossover inhibition. Doris *et al.* showed that oligomerizing active species reduces diffusion through microporous separators, but does not prevent diffusion in mesoporous separators.²⁰ Recently, polymers of intrinsic microporosity,

(PIMs) have gained attention for use in RFBs.^{20–22} PIMs are micro- or nanoporous separators formed by network polymers. Common derivative PIM-1 has an average pore size of less than 2 nm.²² These pores are much smaller than typical RFB separator pores: commonly used separator Daramic, has order 100 nm pores.²³ Pairing PIMs with RAOs allows size selective separation and reduced system cost (Figure 2.2).

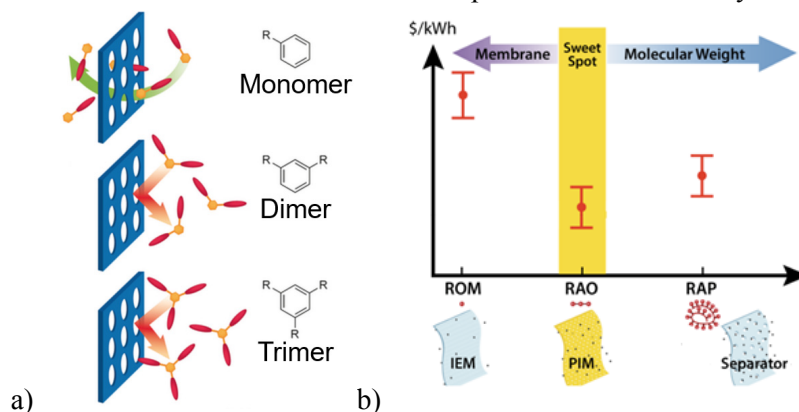


Figure 2.2: Molecular and separator design strategies to prevent crossover. a) Size selectivity. Monomers cross through the separator but dimers and trimers are size excluded.²⁰ b) Comparison of PIMs and other separators. PIMs offer lowest cost and enable use of active species with practical molecular weights.

Despite promising initial results of PIMs in RFBs,^{20,21} there are still challenges that must be overcome before widespread implementation. The first is that PIMs swell in solution, allowing increased crossover over time.²⁰ The second is understanding how electrolyte properties (such as viscosity and active species size) and RFB operating conditions (including current and state of charge) affect transport properties within the separator. The relevant transport mechanisms will be discussed in the next section.

2.3. Losses in Redox Flow Batteries

Redox flow batteries (RFBs) are a promising technology for energy storage, with favorable future state cost and long lifetime [1,2]. RFBs feature independent scaling of energy and power. System power is the product of operating current and voltage. Stack voltage is the sum of the voltages of each element, so stack size dictates system power [3]. Thermodynamic potential of a redox reaction is determined by the Gibb’s free energy of reaction, and this is the ideal voltage of the system (Eq. 1).

$$E = -\frac{\Delta G_{rxn}}{nF} \quad (1)$$

where E is the potential, G is the Gibb’s energy of reaction, n is the number of electrons transferred, and F is Faraday’s constant. Thermodynamic cell potential can only be achieved at equilibrium. Once current is applied, irreversible losses, or overpotentials, will impact the cell potential. There are three main contributions to overpotential: activation (η_{act}), ohmic (η_{ohm}), and concentration (η_{conc}). These losses can be visualized using a polarization curve, wherein cell voltage is plotted as a function of current (Figure 1).

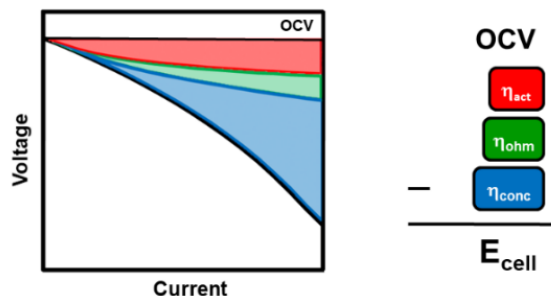


Figure 1: Polarization curve of a RFB. OCV, or open circuit voltage, is the thermodynamic limit, and losses from activation, ohmic, and concentration overpotentials reduce actual cell voltage.

Activation overpotential is the voltage required to drive Faradaic current and depends on the kinetics of the redox reaction and can be described by the Butler-Volmer equation (Eq. 2):

$$i = i_0 \left(e^{\frac{(1-\alpha)nF\eta_{act}}{RT}} - e^{-\frac{\alpha nF\eta_{act}}{RT}} \right) \quad (2)$$

where i is the current density, i_0 is the exchange current density, α is the transfer coefficient (related to the symmetry of the activation energy barrier), and η_{act} is the activation overpotential.

Vanadium RFBs (VRBs) are the most commercialized RFB: however, slow redox kinetics on carbon electrodes result in large activation overpotential, limiting system power [4]. Thermal pretreatment of electrodes can reduce this overpotential. [5] Thermal treatment affects many electrode properties, but which properties contribute to improvements in performance are disputed. Table 1 highlights prior studies of thermally treated electrodes, enhanced electrode properties claimed to be credited for improvements, and percent reduction of total cell resistance. Changes in cell resistance should reflect changes in activation overpotential so long as the cell setup, flowrate, and electrolyte concentration are constant [6].

Table 1: Summary of carbon electrode thermal pre-treatment studies. The electrode property that authors find are enhanced by thermal pretreatment are marked with an X.

Ref.	Temp. (°C)	Functional Groups	Electroactive Surface Area	Graphitic Edge Sites	Hydrophilicity	% Reduction of R_{cell}
[6]	200-500 in air	X				15
[7]	400-610 50 % NH ₃ 50% O ₂	X	X			86
[8]	403-575 in air			X	X	Not reported
[9]	400 42% O ₂ 58% N ₂	X	X			75
[10]	400-600 in air	X		X		Not reported
[11]	600-900 H ₂ O _(v) in air	X				68
[12]	25-200 5% Ozone	X	X			80
[13]	1100-1500 20% CO ₂ 80% N ₂	X	X			60

The variance in properties investigated shows a lack of fundamental understanding as to which govern VRB performance, as well as the complex relationship of parameters; for example, surface functional groups may enhance hydrophilicity [14]. I will study each of these properties as a function of pretreatment temperature and understand the extent each property reduces activation overpotential. This will inform the design of electrodes with properties specific to RFB performance enhancement.

Ohmic overpotential is voltage required to conduct charge, and includes resistance to electron conduction through solids and ion conduction through electrolyte solutions and separators. Electronic resistance is determined by electrical conductivity of solid current collectors, while ionic resistance is governed by ionic conductivity of the electrolyte solution and the battery separator. Ohmic resistance is typically dominated by ionic resistance, as conductivity of cation exchange membranes is order 5 S m⁻¹ [15] and conductivity of vanadium electrolyte is order 50 S m⁻¹ [16], much lower than electronic conductivity of graphite (order 1000 S m⁻¹) [17]. Using values for conductivity, ohmic cell resistance of each component can be estimated (see Appendix A for calculations.)

Concentration overpotential results from diminished active species concentration at an electrode surface compared to bulk solution. This overpotential can be estimated with the limiting current, current

drawn when active species concentration at the electrode surface is zero. Limiting current can be estimated using Rotating Disk Voltammetry. Then concentration overpotential can be calculated (Eq. (4)):

$$\eta_{conc} = \frac{RT}{nF} \ln \left(\frac{i_l}{i_l - i} \right) \quad (4)$$

Concentration overpotential dominates system performance at large current densities, and reducing these losses are particularly important for high power applications. One method is to modify the paths of electrolyte into the porous electrodes, which are dictated by the flow field employed (Figure 2.)

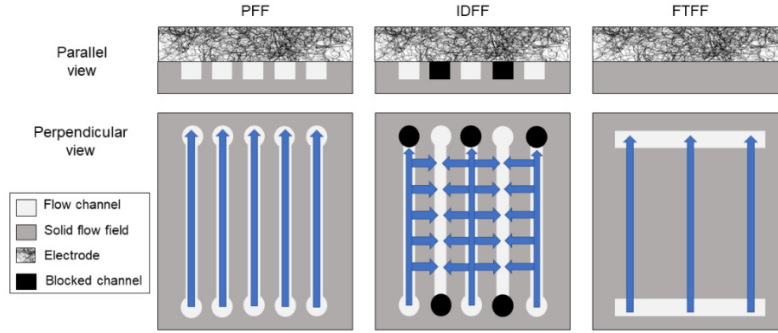


Figure 2: Flow field designs employed in RFBs. Possible flow pathways are indicated by arrows.

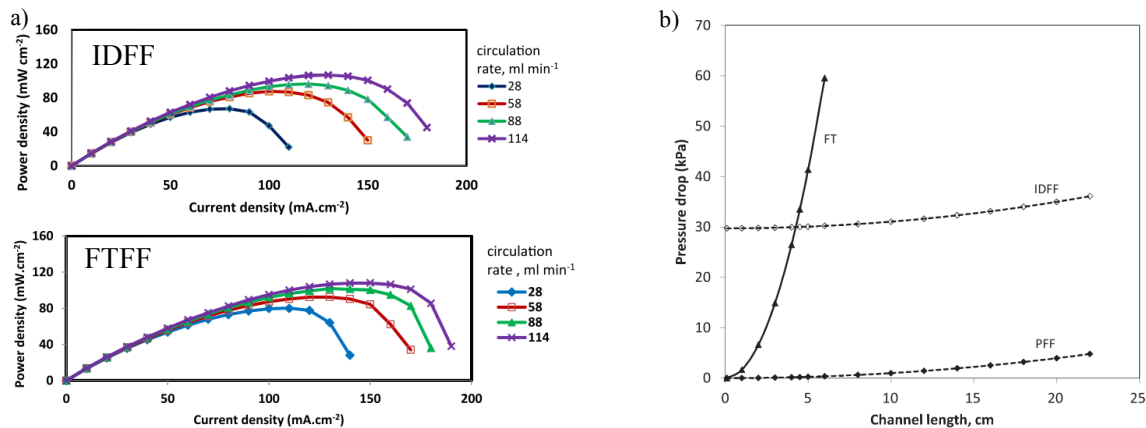
The parallel flow field (PFF) features continuous flow channels from inlet to outlet, and transport into the electrode is dominated by diffusion. The flow-through flow field (FTFF) does not have a direct path from inlet to outlet, and electrolyte is forced to convect into the electrode. FTFFs lead to lower concentration overpotential than the PFF, yet the resulting pressure drop is unfeasible for grid scale systems [19]. The IDFF attempts to merge the positive aspects of these designs: direct paths from inlet to outlet are blocked, forcing convection into the electrode, while channels allow electrolyte to flow unhindered through the length of the flow field, reducing pressure drop. The dimensions of our lab scale flow fields, and equations to estimate representative velocity and pressure drop, are shown in Table 2. Expressions for pressure drop assume fully developed, laminar flow, as well as cylindrical flow channels. The actual channel geometry is rectangular, so these expressions are not an exact solution for my system.

Table 2: Dimensions of lab scale flow fields. Equations that estimate pressure drop and representative velocity through the flow field channels (v_{ch}) and electrode (v_e).

	Channel height (mm)	Channel depth (mm)	Channel length (cm)	Pressure drop [19]	Representative Velocity [19]
PFF	1	0.5	1.6	$\Delta P = \frac{32\mu v_{ch} L_{ch}}{d_n^2}$	$v_{ch} = \frac{Q}{Nwh}$ $v_e = 0$
FTFF	1	0.5	N/A	$\Delta P = \frac{\mu v_e L_{ch}}{k}$	$v_e = \frac{Q}{WL_e}$
IDFF	1	0.5	1.6	$\Delta P = \Delta P_{PFF} \left(1 + \frac{2 + 2 \cosh \zeta}{\zeta \sinh \zeta} \right)$	$v_{ch} = \frac{Q}{Nwh}$ $v_e = \frac{Q}{NL_e L_{ch}}$

The laminar flow assumption is accurate for the systems I utilize: for a typical flow rate of 10 mL min^{-1} , the Reynold's number (Re) of water in a channel is 53. However, assuming fully developed flow may not be accurate. Entrance length for laminar flow is the product of 0.05Re and hydraulic diameter of the channel; for this system entrance length is 1.8 mm, greater than 10% of the total channel length.

The choice of flow field has a large impact on system performance. PFFs have high concentration overpotentials due to poor mass transfer in the absence of forced convection. Darling *et al.* found that PFFs can achieve only 3% of the maximum power density of IDFFs [19]. However, these systems are useful to study diffusion of electrolyte into porous electrodes. IDFFs and FTFFs typically have comparable performance (Figure 3(a)). However, the pressure drop through FTFFs is much larger than IDFFs (Figure 3(b)) [15]. Despite this limitation, FTFFs offer simple conceptual understanding and are the easiest system to model, and I will utilize this system in my research for these purposes.



Reproduced figures provide key background knowledge and are cited appropriately

Figure 3: a) Power density of IDFFs and FTFFs reproduced from Kumar *et al.* [20] b) Measured pressure drop through RFBs utilizing different flow fields. Reproduced from Darling *et al.* [19]

The contribution of system level properties such as pressure drop to concentration overpotential are straightforward to measure experimentally. However, it is often not possible to experimentally determine electrode-scale (such as preferential flow paths through the electrode) and pore-scale (such as difference in active species concentration at the fiber surface compared to bulk solution) contributions to overpotential. To study these multi-scale phenomena, CFD simulations can be utilized. There are several assumptions that are commonly implemented, including incompressible and isothermal fluid, Butler-Volmer redox kinetics, dilute solution approximation, and isotropic mass and charge transfer properties (including resistivity, diffusion coefficients, etc.) Shah *et al.* were the first to implement simulation to study VRB systems [21]. They developed a transient 2D simulation in COMSOL with the assumptions described above and used Darcy's law to describe flow of 1-1.5 M vanadium/4 M H₂SO₄ electrolyte through a porous electrode of 100 cm² area. They showed increasing flow rate decreases concentration overpotential, and that decreasing electrode porosity can increase Coulombic efficiency. This model was simplified by You *et al.* to study cells under steady state conditions [22]. Good agreement with Shah's dynamic model was found, and the steady state simulation showed that decreasing electrode thickness and porosity may lead to more uniform overpotential distribution and that a decrease in local mass transfer coefficients lead to increased overpotential. Knudsen *et al.* and Chen *et al.* implemented 3D flow field geometries in their simulations [23,24]. Knudsen *et al.* simulated flow of liquid bromine through an IDFF using laminar flow equations and through a 400 cm² porous electrode with Darcy's law. They found flow travels most quickly through middle channels of the flow field, and that convection within the electrode in the direction perpendicular to the flow channel is much greater than convection parallel to the channels [23]. Chen *et al.* simulated flow of 0.9 M vanadium through a PFF in the absence of redox reactions using FLUENT software and found electrolyte distribution was greatest in the middle flow field channels [24].

The simulations described above use volume-averaged properties for geometrical features such as electrode permeability, most often from the Kozeny-Carman equation. However, Mostaghimi *et al.* used high resolution images of porous media to calculate permeability, and found the Kozeny-Carman equation

can overestimate permeability by a factor of 10 [25]. Qiu *et al.* compared the volume averaged model of You *et al.* with Lattice-Boltzmann simulations of flow through micro-CT electrode images [26]. Good agreement was found for system level properties such as cell polarization, indicating the Kozeny-Carman equation provides a reasonable estimate of carbon electrode permeability. Additionally, resolving geometrical features elucidated how concentration overpotential varies along fiber surfaces, and it was seen that electrode overpotential is greatest near the current collector and decreases along the fiber length.

System energy is determined by the product of cell voltage and charge capacity of the system. Charge capacity is a function of electrolyte volume and concentration and can be calculated using Eq. 5:

$$Q_{chg} = nFC_{actives}V_{electrolyte} \quad (5)$$

where C is concentration of active species and V is electrolyte volume. Therefore, energy capacity of a RFB system can be set by the quantity of electrolyte. System energy capacity is less than the theoretical limit due to crossover of active species from one electrolyte to another. Crossed over ions react with ions in the opposite half-cell, causing self-discharge. Ideal flow battery separators should prevent crossover of active species while allowing ions of the supporting salt to pass through unhindered. Ion Exchange Membranes (IEMs) are most commonly utilized in RFBs, but these separators increase system cost, motivating research into alternatives such as Polymers of Intrinsic Microporosity (PIMs) or size selective porous separators. Table 3 shows properties of commonly utilized separators for RFB applications.

Table 3: Properties of commonly utilized RFB separators.

Separator	Type	Thickness (μm)	Pore Size (nm)	Ionic Conductivity (mS cm^{-1})
Nafion 117	IEM	183 [27]	2 [28]	60.2 [29]
Nafion 212	IEM	50.8 [30]	4 [31]	69.7 [29]
PIM-1	PIM	> 10	2 [32]	0.4 [32]
Daramic 175	Porous Separator	250 [33]	100 [33]	1 [33]
Celgard 2500	Porous Separator	25 [34]	43 [34]	2.2 [32]

Transport of active species through a separator can be separated into contributions from diffusion, convection, and electromigration, according to the Nernst-Planck equation [35] (Eq. 6):

$$N_i = -D_i \nabla C_i + v_i C_i - z_i u_i F C_i \nabla \phi \quad (6)$$

Diffusion coefficients of active species within a separator can be measured *ex-situ* in an H-cell, wherein solution containing active species and supporting salt is separated from solution containing equal concentration of supporting salt but no active species. Measuring concentration of active species in the blank solution over time allows the calculation of diffusion coefficient from Fick's law. Convective crossover can be separated into hydraulic pressure driven convection and electro-osmosis. These contributions to intra-membrane velocity v^m can be described by the Schlogl equation [36] (Eq. 7):

$$v^m = -\frac{\kappa_p}{\mu} \nabla p - \frac{\kappa_\phi}{\mu} C_m F (\nabla \phi_l^m + \nabla \phi_{diff}^m) \quad (7)$$

where κ_p and κ_ϕ are hydraulic and electrokinetic permeability, respectively; C_m is concentration of charged groups in the membrane; ϕ_l^m is liquid potential across the membrane; and ϕ_{diff}^m is effective diffusion

potential that accounts for viscous drag of ion diffusion and can be calculated from ion diffusivity and the effective membrane conductivity [37]. Convection is dominated by electro-osmotic contributions [38–40]; however, Knehr *et al.* utilized a 2D model of vanadium crossover to show that osmotic pressure contributions to crossover are non-negligible [41]. The model assumes 10 cm² active area, 1.04 M vanadium/5.04 M H₂SO₄ electrolyte concentration, Butler-Volmer kinetics, and dilute electrolyte. This model is also the first reported that accounts for transport of all electrolyte species (vanadium ions, protons, sulfate ions, and water molecules) through the separator [36]. The model also accounts for changes in solution viscosity during cycling, which affects osmotic pressure differentials. Two types of flow conditions are considered: constant flow rate, where the volumetric flow rate of both electrolytes are equal, and constant pressure, where the pressure on both sides of the half-cell are equal. In both cases, the net transfer of vanadium ions is from the positive to the negative half-cell. However, the constant flow rate condition induced a 10% greater change in vanadium ion concentration over 35 cycles due to crossover as compared to the constant pressure condition. These results highlight the usefulness of CFD simulations to study contributions to crossover. Agar *et al.* [42] utilized the Knehr simulation [36] to study crossover contributions in a sulfonated Radel membrane, a less expensive alternative to the commonly used Nafion membrane. They found vanadium crossover in Nafion is dominated by diffusion, whereas crossover in s-Radel is convection dominated. This work shows that the most effective strategies to reduce crossover will differ greatly depending on the separator employed. Oh *et al.* utilized a 3D model of Darcian flow within electrodes to investigate vanadium ion crossover at different states of charge [43]. Their model uses 4 cm² active area and 1.1 M vanadium/5 M H₂SO₄ electrolyte. They found the crossover of vanadium ions is much greater at higher current densities due to a greater migrative crossover [39]. Despite the progress made with simulations, contributions to electrolyte crossover have not been deconvoluted experimentally. One of the major goals of my thesis work will be to utilize a RFB system inspired by the work of Sing *et al.* [44] to study contributions of separate transport mechanisms to crossover. This experimental work will complement the results from CFD simulations, and can be used to inform the validity of the assumptions used in these simulations and improve the accuracy of the models.

Research Plan

3. Research Plan

The previous section outlined the importance of transport mechanisms within RFBs and prior work that studied these processes. However, increase efficacy of RFB transport, individual transport mechanisms must be separated and evaluated. To study individual transport mechanisms and to evaluate resulting changes in cell performance, my thesis work will be centered on two key questions:

1. What is the role of surface composition, morphology, and electrolyte properties on transport within porous electrodes?
2. What are the impacts of diffusion, convection, and electromigration on crossover and subsequent flow cell performance and how can these effects be experimentally deconvoluted?

To answer question (1), I will begin by varying electrode morphology, characterizing these changes, and observing effects on RFB performance (Section 3.1). I will further study transport within porous electrodes by using simulations and imaging to observe transport of electrolyte over the entire electrode area (Section 3.2). The effects of electrolyte properties such as [REDACTED] on transport within electrodes will be studied (Section 3.3.) The effect of [REDACTED] on crossover will also be determined (Section 3.3), touching on question (2). Question (2) will be fully addressed by designing a system to study individual transport mechanisms that contribute to active species crossover (Section 3.4).

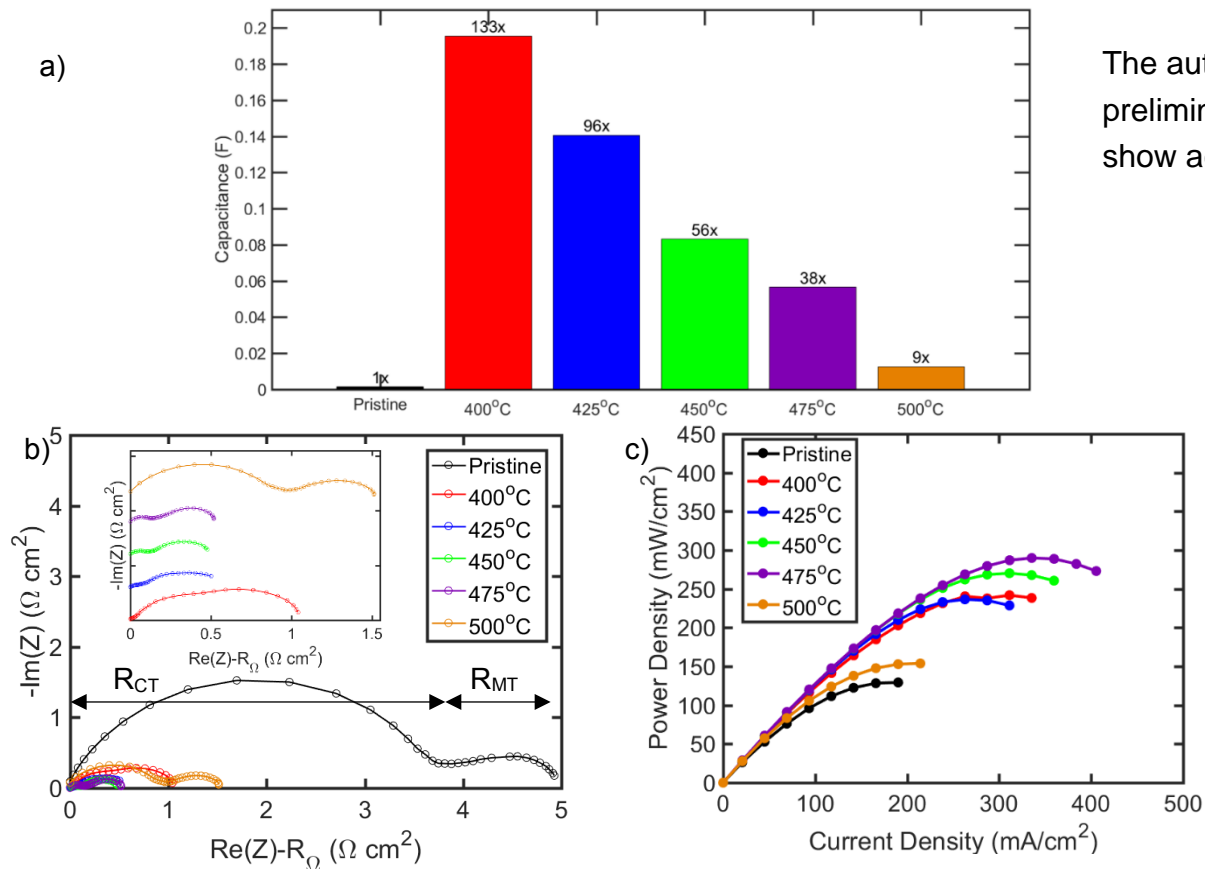
These questions remind the reader of the specific aims

3.1. Understanding Role of Electrode Morphology on Performance

The research plan uses sections to guide the audience through the document

Carbon materials commonly utilized as RFB electrodes have diverse morphologies. Further morphology changes are possible via pre-treatment methods such as thermal treatment. What effects do morphology changes have on transport mechanisms in porous electrodes? What properties will lead to the most effective transport, and therefore best performance? As described in Section 2.3.1., pre-treatment of carbon electrodes is an active research area in the field. However, most literature primarily focuses on describing performance gains rather than understanding the underlying chemical and morphological properties that lead to these improvements. In my thesis work, I will study electrode properties via ex situ and in situ characterization and use the results to explain changes in flow battery performance. This understanding will be necessary to fully characterize transport within porous electrodes.

To begin to investigate electrode morphology, this semester I have undertaken an in-depth study of heat treated Sigracet SGL 29AA carbon paper electrodes. As discussed above, carbon papers are more viable for use in large scale RFBs but are less studied than felts. I have treated samples at temperatures ranging from 400-500°C in increments of 25°C for use in VRB systems. I have characterized electrodes using ex situ techniques including XPS, Raman spectroscopy, Scanning Electron Microscopy (SEM), capacitance measurements, and wetting properties. I have also studied in situ flow cell performance using electrochemical impedance spectroscopy (EIS), polarization, and constant current cycling. Vanadium electrolyte has allowed me to study both kinetic and transport effect of electrode morphology. This study an ideal project to begin my thesis work: I learned how to build consistent flow cells and became familiar with characterization equipment available through MIT and at Harvard's CNS. Through this work, I discovered that there is a complex relationship between electrochemical surface area and mass transport resistance, both of which affect flow cell performance (Figure 3.1).



The author uses preliminary data to show acquired skills

Figure 3.1: Characterization and performance of heat treated SGL 29AA carbon paper electrodes. a) Capacitance measured from CV. Labels show magnitude compared to pristine samples. b) Nyquist plots

derived from EIS. The first arc corresponds to charge transfer resistance (R_{CT}), while the second arc represents mass transfer resistance (R_{MT}). c) Power output of cells measured via polarization.

As seen in Figure 3.1(a), electrodes treated at 400°C have the highest increase in capacitance, and therefore the highest electrochemically active surface area.⁴⁶ However, electrodes treated at 450 and 475°C outperform these electrodes (Figure 3.1(c)). This discrepancy can be explained by lower charge transfer and mass transfer resistance of the 450 and 475°C electrodes, as seen in Figure 3.1(b). The resistance is a function of morphological properties; lower resistance despite less reactive surface area shows the importance of complete electrode characterization. The specific advantages of electrodes treated at 475°C are increased oxygen functional groups on the electrode surface, faster wetting dynamics, and larger pore size, the results of which can be seen in Appendix B1.

By studying the effect of thermal treatment on carbon papers, we have begun to characterize morphology changes and how these changes affect flow cell performance. There are still many questions left to address. For example, will morphology changes have the same effect in electrodes of different thicknesses? And will electrode morphology be equally impactful in systems with faster active species kinetics? To answer these questions I will continue to characterize the morphology of each electrode I investigate in this thesis work, and I will investigate the effect in kinetically facile NAqRFB systems.

Although coupling ex situ characterization with flow cell studies is useful to study the impact of electrode properties on cell performance, it is difficult to study the fundamental mechanisms that lead to these improvements. To fully characterize transport within electrodes I will apply a combination of imaging and modeling techniques, described in the next section.

3.2. Transport at Each Position in Porous Electrodes

In situ experimental studies are necessary to accurately characterize transport within an electrode. However, values for mass transfer coefficient and other relevant variables extracted from flow cell testing are bulk properties, and averaging over the entire electrode area causes important details to be lost. Are bulk properties adequate to characterize transport in RFBs? To fully characterize transport properties, we must study flow across entire electrode areas. A technique that will allow us to study this flow is CFD simulation. However, CFD is extremely computationally expensive, making it difficult to simulate a representative electrode volume (REV). Determining the REV is also a challenge. In the case of carbon papers, there is no REV in the through-plane (the thinnest dimension, Fig. 3.2), as papers are too thin.⁴⁷ Therefore, simulations alone are not sufficient. Imaging is a powerful tool that, coupled with simulations, can accurately describe transport at each position within a porous electrode.

The imaging techniques we are interested in are X-Ray Tomographic Microscopy (XTM) and [REDACTED] XTM acquires high resolution (1 μm -1 nm) images, capturing detailed 3-D microstructures. However, X-rays offer poor contrast between carbon and electrolytes, and acquisition times are too great to observe dynamics. Consequently, we will simulate flow through microstructures obtained from tomography. To study active species flow experimentally, we will utilize [REDACTED]

[REDACTED] One example of how this coupling can be advantageous is to inform CFD simulations. Typically, a no-flux condition at the current collector and at the separator are assumed.^{49,50} By imaging flow in the in-plane direction, we can determine whether this boundary condition is accurate. Imaging in the through-plane direction can describe flow patterns through flow fields. This will offer a particularly useful addition to CFD models, as simulating flow field area is too computationally expensive. By determining active species

concentration through different flow fields, we can design geometries that will maximize distribution and minimize concentration overpotentials, leading to improved battery performance.

This work will be possible via collaboration. [REDACTED]

[REDACTED]

[REDACTED] We will work simultaneously with Professor Nigel Brandon at Imperial College London, who produces high resolution images of porous electrodes using XTM. The Brushett and Brandon groups have been awarded a 2017-2018 MISTI travel grant for collaboration. Their group has imaged electrode samples we sent, and we will soon begin CFD simulations.

By simultaneously developing these collaborations, we can fully characterize in situ active species transport over the full area of RFB electrodes.

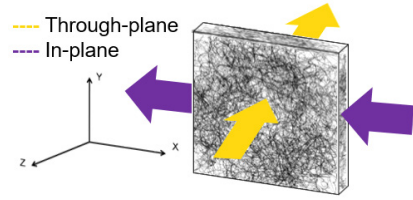


Figure 3.2: In-plane and through-plane orientation of electrodes.

3.3. [REDACTED]

[REDACTED]

[REDACTED]

[REDACTED]

[REDACTED]

[REDACTED]

[REDACTED]

3.4. Distinct Mass Transport Mechanisms in Operating Flow Cells

3.4.1. System Design and Validation

To fully characterize mass transport within a RFB, we must develop methods to deconvolute contributions of mass transport mechanisms during cell operation. We are particularly interested in in situ measurements to quantify contributions from convection and electromigration, which are difficult to measure in isolation. To this end, I will utilize a crossover flow cell similar to that employed in David Sing's thesis work at UT Austin.⁵³ This cell enables direct crossover measurements in situ and as a function of different transport mechanisms. An overview of the cell design can be seen in Figure 3.6.

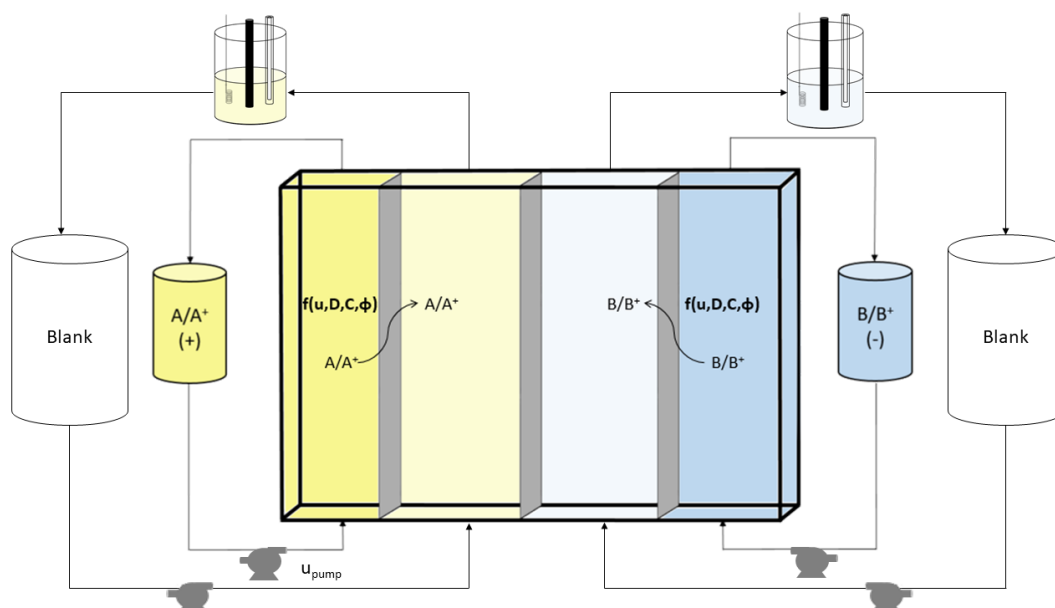


Figure 3.6: Crossover flow cell configuration. Active species is pumped to the outer chambers which function as typical half-cells. Blank solution (salt and solvent without active species) flows through the inner chambers. Active species crossover is measured with voltammetry or other techniques.

This flow cell design, called the crossover cell, utilizes three separators and four electrolyte chambers. The two chambers on the outside of the cell are the normal negative and positive electrodes of a full cell flow battery, and will contain the electrodes and separators of interest. Solvent and supporting salt with no active species, or “blank” solution, is pumped through the inner chambers. The supporting salt will be present in excess in both the blank solution and electrolyte, so osmotic pressure differences should be negligible and crossover from the negative and positive half-cell to the inner chambers should be similar to crossover from one half cell to another in a full cell configuration. A thicker separator will be used in the middle of the cell to make crossover through the inner chambers negligible.⁵³ I will run voltammetry on the blank solution exiting the cell with a UME to determine the extent of active species crossover and the electrolyte state of charge. However, this technique cannot be used continuously nor in situ in our lab facilities, as a separate cell set up with constant concentration must be used. As testing progresses, I will investigate continuous measurements such as UV-Vis spectroscopy or conductivity.

Sing's work provides a basis for the cell design, yet there are still many reactor design challenges that must be addressed. The flow fields in the inner chambers must allow the sufficient contact of the blank

solution with both the separator of interest and central separator to maintain electroneutrality. The design must allow unhindered crossover of the active species, but utilize a zero-gap architecture to maintain reasonable ohmic resistance.⁵⁴ I will address these and other challenges using my knowledge of engineering and reactor design obtained through classes and lab experience.

Once a working crossover cell has been developed, I will confirm that measurements are comparable to a full flow cell. Polarization and cycling experiments will determine if performance characteristics of the crossover cell are comparable to a full cell. EIS will determine whether the resistance contributions are analogous. I expect the ohmic resistance will be higher within the crossover cell, as each flow field and separator contributes internal resistance. Though this will increase cell overpotential, this effect is easily measured and accounted for. By understanding the performance variations, we can identify and study mass transfer characteristics independently of structural differences.

I anticipate that cell design and validation will be an iterative process. For example, I will determine which flow fields and electrodes give performance most similar to that of a full cell and modify the design accordingly. I expect this process to continue throughout my thesis work.

3.4.2. Mechanistic Contributions to Electrolyte Crossover

Once crossover cell design is complete and we are confident collected data will be sound, we can begin to utilize the cell to study crossover in situ. First, we must choose a mass transport characteristic to isolate. Diffusion is the most straightforward transport mechanism to separate and can be measured ex situ, as diffusion in bulk solution can easily be measured using well-established voltammetry techniques. Diffusion through a separator can be measured using an H-Cell, wherein the active species of interest is placed on one side and a blank solution containing the same solvent and salt concentration is placed on the other. The two sides of the cell are separated by the separator of interest. Using voltammetry and a UME or UV-Vis spectroscopy, the change in concentration of active species over time can be measured, giving an estimate for diffusion coefficient of active species through the separator. Diffusion through the porous electrodes will be estimated from CFD simulations (see Section 3.2).

Since diffusive contributions to crossover can be determined ex situ, the logical choice is to begin by studying the effect of convection on crossover. Conducting these measurements in the absence of current will eliminate migration effects. In flow fields where the channels are continuous, such as PFFs, the effective electrolyte velocity is zero and transport within the electrode is diffusion dominated. Therefore, we expect that crossover will be independent of convection. However, in electrodes with blocked channels, Pe is large and electrode transport is convection dominated, so we expect that convection has a large effect on crossover. The exact relationship between convective and diffusive crossover at different flow rates, and subsequently different Peclet numbers, will be determined. In doing so we will answer the following question: How will crossover rates in diffusion and convection controlled regimes differ? I will investigate this question for microporous separators as well as IEMs. These studies will allow me to solve the discrepancy outlined in Section 2.3.2., namely that transport in IEMs is widely believed to be diffusion and migration dominated, yet the model developed by Knehr *et al.* indicates pressure-driven convection contributes significantly to vanadium ion crossover.⁴²

Once we have isolated crossover contributions from diffusion and osmotic convection, we can study the impact of applied potential. In the presence of an electric field, electromigration will cause positively charged ions to move in the direction of the applied electric field and negatively charged ions to move in the opposite direction. Neutral species will also move via electro-osmotic convection. Pressure-driven convective and diffusive contributions should be electric field independent.⁵⁵ The question to be answered is, to what extent does applied potential influence crossover? By measuring the convective contribution to crossover both with and without applied potential, we can determine the contribution of hydraulic convection to crossover and solve the discrepancy outlined in Section 2.3.2.

Next, the effect of battery state of charge (SOC) on crossover will be considered. SOC should influence electromigration, which is oxidation state dependent. SOC may also affect convection and diffusion, as different oxidation states have altered physical properties such as viscosity and molecular radius. Overpotential causes cell voltage to vary during cycling, so crossover rate may also change during cell cycling. These expectations lead to the questions: What is the influence of SOC on transport mechanisms at steady state? How do these mechanisms change when currents are applied?

Through these studies, I will identify the dominant crossover mechanisms as a function of operating conditions, electrolyte properties, and electrode morphology. The results can be used to determine optimal cell configuration and conditions to prevent crossover. This understanding will enable us to recommend RFB configurations that will lead to highest possible system efficiency, bringing the field one step closer to developing commercially viable flow batteries for grid scale energy storage.

Safety

4. Safety

The most potentially dangerous component of a flow battery is the electrolyte. VRBs typically operate in acidic conditions, while NAqRFBs utilize toxic organic solvents. To prevent exposure, proper PPE will be worn at all times, including: flame- and chemical-resistant lab pants, flame- and chemical-resistant lab coat, nitrile gloves, and safety glasses. When working with organic solvents for non-aqueous systems, I will substitute nitrile gloves for more resistant latex.⁵⁶ Electrolyte tanks and operating flow batteries will be kept in secondary containment to contain any leaks that may occur. Acidic electrolyte will be disposed in an acid waste stream located in a designated acid fume hood, while organics will be disposed in an organic waste stream located in a fume hood designated for organics. Experiments utilizing hazardous organic solvents such as acetonitrile will either be performed in a glovebox or fume hood designated for organic use. Non-aqueous electrolytes typically utilize fluorine-containing functional groups that have the potential form hydrofluoric acid in water. Flow cell components will be thoroughly rinsed and sonicated in acetone to remove all electrolyte species before further sonication in water.

Driving electrochemical reactions necessitates the use of a potentiostat, a source of potentially hazardous current flow. Operating currents used for my experiments are in the range of 5 – 500 mA. Current can cause serious injury at 10 mA and be fatal above 100 mA.⁵⁷ I will never grip electrical leads when the potentiostat is powered on. I will ensure that conductors such as wire leads are insulated with electrical tape. To prevent injury to others, I will place signs stating drawn current near each experiment.

The Safety section identifies key hazards of the experiments and describes how they will be mitigated

Timeline

5. Timeline The timeline provides detailed tasks for each semester

The timeline presented is a rough schedule towards completing my thesis work. This schedule will likely change as research progresses. Note that I will be attending Practice School in Spring 2018. However, I have also highlighted the oligomerization projects, as I am planning on training an undergraduate to continue working on these projects while I am away.

Table 5.1: Proposed thesis timeline. Tasks are shown as rows, while semesters are plotted as columns. Intended first author publication topics are marked with an asterisk.

	2017	2018			2019			2020			2021		
Thesis Task	Fall	Spring	Summer	Fall	Spring	Summer	Fall	Spring	Summer	Fall	Spring	Summer	Fall
Heat Treatment Morphology*													
██████████													
██████████████████													
Practice School													
XTM and CFD Simulations													
██████████													
Flow Cell Design													
Convective vs. Diffusive Crossover*													
Effect of Electromigration and SOC on crossover*													
Thesis Defense													

* Indicates 1st author publication topic

References

6. References

1. I. Gyuk et al., *Grid Energy Storage*, (2013).
2. N. Pour et al., *J. Phys. Chem. C*, **119**, 5311–5318 (2015).
3. P. A. Boettcher et al., *J. Electrochem. Soc.*, **163**, 5244–5252 (2016).
4. R. Darling, K. Gallagher, W. Xie, L. Su, and F. Brushett, *J. Electrochem. Soc.*, **163**, A5029–A5040 (2016) <http://jes.ecsdl.org/lookup/doi/10.1149/2.0051601jes>.
5. K. J. Kim et al., *J. Mater. Chem. A*, **3**, 16913–16933 (2015) <http://xlink.rsc.org/?DOI=C5TA02613J>.
6. W. Wang et al., *Adv. Funct. Mater.*, **23**, 970–986 (2013).
7. D. Rastler, *Electric Energy Storage Technology Options: A White Paper Primer on Applications, Costs and Benefits*, p. 1-170, (2010) <http://large.stanford.edu/courses/2012/ph240/doshay1/docs/EPRI.pdf>.
8. M. L. Perry and A. Z. Weber, *J. Electrochem. Soc.*, **163**, A5064–A5067 (2016) <http://jes.ecsdl.org/lookup/doi/10.1149/2.0101601jes>.
9. L. Su, J. A. Kowalski, K. J. Carrol, and F. R. Brushett, *Recent Developments and Trends in Redox Flow Batteries*, p. 262-269, (2011).
10. A. Crawford et al., *J. Power Sources*, **293**, 388–399 (2015) <http://dx.doi.org/10.1016/j.jpowsour.2015.05.066>.
11. C. Choi et al., *Renew. Sustain. Energy Rev.*, **69**, 263–274 (2017) <http://dx.doi.org/10.1016/j.rser.2016.11.188>.
12. M. Skyllas-Kazacos, L. Cao, M. Kazacos, N. Kausar, and A. Mousa, *ChemSusChem*, **9**, 1521–1543 (2016).
13. Y. Zhou et al., *RSC Adv.*, **7**, 19425–19433 (2017) <http://xlink.rsc.org/?DOI=C7RA00294G>.
14. K. A. Mauritz and R. B. Moore, *Chem. Rev.*, **104**, 4535–4585 (2004).
15. K. Oh, S. Won, and H. Ju, *Electrochim. Acta*, **181**, 238–247 (2015) <http://dx.doi.org/10.1016/j.electacta.2015.03.012>.
16. J. T. Clement, D. S. Aaron, and M. M. Mench, *J. Electrochem. Soc.*, **163**, A5220–A5228 (2016) <http://jes.ecsdl.org/lookup/doi/10.1149/2.0241601jes>.
17. D. D. Lide, *CRC Handb. Chem. Physics, 87th Ed.*, 1–10 (2005) [papers3://publication/uuid/F8394DAA-9AE4-4AA2-87A7-39F227EBD02A](https://pubs3://publication/uuid/F8394DAA-9AE4-4AA2-87A7-39F227EBD02A).
18. L. Su et al., *Electrochim. Acta*, **246**, 251–258 (2017) <http://dx.doi.org/10.1016/j.electacta.2017.05.167>.
19. H. Prifti, A. Parasuraman, S. Winardi, T. M. Lim, and M. Skyllas-kazacos, *Membranes (Basel)*, **2**, 275–306 (2012).
20. S. E. Doris et al., *Angew. Chemie - Int. Ed.*, **56**, 1595–1599 (2017).
21. C. Li et al., *Nano Lett.*, **15**, 5724–5729 (2015).
22. N. B. McKeown and P. M. Budd, *Chem. Soc. Rev.*, **35**, 675 (2006) <http://xlink.rsc.org/?DOI=b600349d>.
23. J. D. Milshtein, T. Moore, and L. Thompson, *ChemSusChem* (2017).
24. W. Deen, *Analysis of Transport Phenomena*, 2nd ed., p. 574, Oxford University Press, New York, (2012).

25. R. M. Darling and M. L. Perry, *J. Electrochem. Soc.*, **161**, A1381–A1387 (2014).
26. B. Sun and M. Skyllas-Kazacos, *Electrochim. Acta*, **37**, 1253–1260 (1992) <http://linkinghub.elsevier.com/retrieve/pii/001346869285064R>.
27. L. J. Small et al., *Synthesis via Chemical Reduction of V₂O₅ in Aqueous HCl and H₂SO₄*, Albuquerque, New Mexico, (2017).
28. A. Khazaeli, A. Vatani, N. Tahouni, and M. H. Panjeshahi, *J. Power Sources*, **293**, 599–612 (2015) <http://dx.doi.org/10.1016/j.jpowsour.2015.05.100>.
29. W. Xie, R. M. Darling, and M. L. Perry, *J. Electrochem. Soc.*, **163**, A5084–A5089 (2016) <http://jes.ecsdl.org/lookup/doi/10.1149/2.0111601jes>.
30. M. H. Chakrabarti et al., *J. Power Sources*, **253**, 150–166 (2014).
31. O. Nibel et al., *J. Electrochem. Soc.*, **164**, A1608–A1615 (2017) <http://jes.ecsdl.org/lookup/doi/10.1149/2.1081707jes>.
32. D. Kil, H. J. Lee, S. Park, S. Kim, and H. Kim, *J. Electrochem. Soc.*, **164**, A3011–A3017 (2017).
33. D. M. Kabtamu, J. Y. Chen, Y. C. Chang, and C. H. Wang, *J. Power Sources*, **341**, 270–279 (2017) <http://dx.doi.org/10.1016/j.jpowsour.2016.12.004>.
34. D. Aaron et al., *J. Power Sources*, **366**, 241–248 (2017) <https://doi.org/10.1016/j.jpowsour.2017.08.108>.
35. S. Kumar and S. Jayanti, *J. Power Sources*, **307**, 782–787 (2016) <http://dx.doi.org/10.1016/j.jpowsour.2016.01.048>.
36. J. Houser, J. Clement, A. Pezeshki, and M. M. Mench, *J. Power Sources*, **302**, 369–377 (2016) <http://dx.doi.org/10.1016/j.jpowsour.2015.09.095>.
37. C. R. Dennison et al., *J. Electrochem. Soc.*, **163**, A5163–A5169 (2016).
38. SGL Group, (2016) http://www.sglgroup.com/cms/_common/downloads/products/product-groups/su/fuel-cell-components/White-Paper-SIGRACET-GDL-for-Fuel-Cells.pdf.
39. E. Agar, K. W. Knehr, D. Chen, M. A. Hickner, and E. C. Kumbur, *Electrochim. Acta*, **98**, 66–74 (2013) <http://dx.doi.org/10.1016/j.electacta.2013.03.030>.
40. C. Sun, J. Chen, H. Zhang, X. Han, and Q. Luo, *J. Power Sources* Sun, C., Chen, J., Zhang, H., Han, X., Luo, Q. (2010). *Investig. Transf. water vanadium ions across Nafion Membr. an Oper. vanadium redox flow Batter. J. Power Sources*, 195(3), 890–897. <https://doi.org/10.1016/j.jpowsour.2010.03.030>, **195**, 890–897 (2010).
41. X.-G. Yang, Q. Ye, P. Cheng, and T. S. Zhao, *Appl. Energy*, **145**, 306–319 (2015) <http://www.sciencedirect.com/science/article/pii/S0306261915002159>.
42. K. W. Knehr and E. C. Kumbur, *Electrochem. commun.*, **23**, 76–79 (2012) <http://dx.doi.org/10.1016/j.elecom.2012.07.008>.
43. B. Li et al., *ChemSusChem*, **7**, 577–584 (2014).
44. X. L. Zhou, T. S. Zhao, L. An, Y. K. Zeng, and L. Wei, *J. Power Sources*, **327**, 1–7 (2016).
45. X. Wei et al., *Polym. Rev.*, **55**, 247–272 (2015).
46. C. N. Sun, F. M. Delnick, L. Baggetto, G. M. Veith, and T. A. Zawodzinski, *J. Power Sources*, **248**, 560–564 (2014) <http://dx.doi.org/10.1016/j.jpowsour.2013.09.125>.

47. P. A. Garcia-Salaberri et al., in *232nd Electrochemical Society Conference*, (2017).
48. N. Kardjilov, I. Manke, A. Hilger, M. Strobl, and J. Banhart, *Mater. Today*, **14**, 248–256 (2011) [http://dx.doi.org/10.1016/S1369-7021\(11\)70139-0](http://dx.doi.org/10.1016/S1369-7021(11)70139-0).
49. M. D. R. Kok, A. Khalifa, and J. T. Gostick, *J. Electrochem. Soc.*, **163**, A1408–A1419 (2016) <http://jes.ecsdl.org/lookup/doi/10.1149/2.1281607jes>.
50. M. Al-yasiri and J. Park, *J. Electrochem. Soc.*, **164**, 1970–1982 (2017).
51. X. Wei, W. Xu, M. Vijayakumar, L. Cosimbescu, and T. Liu, *Adv. Mater.*, **26**, 7649–7653 (2014).
52. W. Deen, **33**, 1409–1425 (1987).
53. D. C. Sing and J. P. Meyers, in, vol. 50, p. 61–72 (2013).
54. D. S. Aaron et al., *J. Power Sources*, **206**, 450–453 (2012) <http://dx.doi.org/10.1016/j.jpowsour.2011.12.026>.
55. R. M. Darling, A. Z. Weber, M. C. Tucker, and M. L. Perry, *J. Electrochem. Soc.*, **163**, 5014–5022 (2016).
56. Cole-Parmer, (2017) <http://www.coleparmer.com/Chemical-Resistance>.
57. Elmwood Electric, Inc., (1987) https://www.physics.ohio-state.edu/~p616/safety/fatal_current.html.
58. Z. Jiang, K. Klyukin, and V. Alexandrov, *J. Chem. Phys.*, **145**, 114303 (2016).